

**Ravi Balasubramanian**<sup>1</sup>

School of Mechanical, Industrial,  
and Manufacturing Engineering,  
Oregon State University,  
Corvallis, OR 97331  
e-mail: ravi.balasubramanian@oregonstate.edu

**Joseph T. Belter**

e-mail: joseph.belter@yale.edu

**Aaron M. Dollar**

e-mail: aaron.dollar@yale.edu

Department of Mechanical Engineering,  
Yale University,  
New Haven, CT 06520

# Disturbance Response of Two-Link Underactuated Serial-Link Chains

*In an attempt to improve the performance of underactuated robotic hands in grasping, we investigate the influence of the underlying coupling mechanism on the robustness of underactuated hands to external disturbance. The coupling mechanisms used in underactuated mechanisms can be divided into two main classes based on the self-adaptive transmission used to route actuation to the degrees of freedom, namely single-acting and double-acting transmissions. The kinematic coupling constraint is always active in double-acting mechanisms, while there are specific combinations of external disturbances and mechanism parameters that render the constraint inactive in single-acting mechanisms. This paper identifies unique behaviors in terms of mechanism reconfiguration and variation in grasping contact forces that result from the underactuated hand's response to external disturbance forces and show that these behaviors are a function of the coupling mechanism, actuation mode, and contact constraints. We then present an analysis of how these behaviors influence grasping ability of the hand and discuss implications for underactuated hand design and operation. [DOI: 10.1115/1.4006279]*

## 1 Introduction

There has long been a desire to minimize the number of actuators in robotic hands due to the constraints on size and mass as well as the greater reliability and lower cost of simplified mechanical construction. This has been accomplished by coupling the motion of multiple joints, with many designs having fewer actuators than degrees of freedom. Such robotic hands, termed “underactuated,” have shown significant benefits in grasping applications due to the passive adaptability between the degrees of freedom; that is, under certain conditions the unconstrained freedoms afford these hands an ability to conform to the environment shape without any sensing. While the performance and design of the underactuated hands when driven through internal actuation have been analyzed in prior work [1–5], the behavior of these hands in the presence of external disturbance forces is still not well understood.

Disturbance forces can arise in several situations, including unplanned collisions, vibration or acceleration of the base, or the varying force applied by another finger, often transmitted through the object. Such disturbance forces can cause a finger to reconfigure and also affect the internal force in the coupling mechanism and the contact forces maintained with an object, potentially destabilizing the grasp. A grasp's ability to resist a force acting on an object has been studied before for a specific class of underactuated mechanisms, where the coupling constraint between the actuator and the degrees of freedom is always active, by constructing an energy landscape as the object is pulled in different directions [6]. However, the above study did not focus on the mechanism's reconfiguration due to the disturbance force when the hand is operated in different control modes. Also, there exist underactuated mechanisms where the coupling constraint can become inactive under certain conditions, and these mechanisms exhibit a significantly different response to external disturbances.

The two classes of transmission mechanisms we refer to are single-acting mechanisms and double-acting mechanisms. Single-acting mechanisms control either the flexion or extension of the

finger (see Fig. 1(a)). This is achieved using an actuator that can only pull (for example, a single cable routing) or push (for example, a plunger), and the reverse motion is achieved using springs. Examples of robotic hands with single-acting mechanisms include the SDM [1], Balance Bar [7], and 100G robotic hands [8].

In contrast, double-acting mechanisms control both the flexion and the extension motion of the fingers (see Fig. 1(c)). This is achieved through different methods, such as four-bar linkages, double cable routing, or gears. Examples of robotic hands with double-acting mechanisms include the Laval Hands [9,10], SPRING [11], Southampton [12], Graspar [13], BarrettHand [14], and Obrero [15] robotic hands.

The key difference between the two classes of underactuated mechanisms is that under certain conditions, the single-acting mechanism's coupling constraint can become inactive. This happens, for example, when the cable becomes slack due to external disturbances (see Fig. 1(b)). In contrast, the constraint is always active in a double-acting mechanism. To our knowledge, prior work has studied underactuated mechanisms only when the constraint is active.

The primary contribution of this paper is analyzing the disturbance response of single-acting underactuated mechanisms when the coupling constraint becomes inactive, focusing on the mechanism's reconfiguration and the variation in contact and actuator forces due to the disturbance. We first present a framework for studying the disturbance response of underactuated hands, taking into consideration the kinematics of the coupling mechanism, contact constraints, and actuator control modes. Then, in Sec. 3, we present the results from an analysis of the disturbance response of two-link single-acting and double-acting underactuated fingers under different conditions. Finally, in Sec. 4, we present a discussion of the interesting behaviors arising from the combination of control modes and the coupling mechanisms and how understanding the entire parameter subspace can inform the design and operation of underactuated hands. Portions of this paper have been published in Refs. [16,17], but those papers did not focus on the disturbance response of underactuated mechanisms in the presence of object contact.

## 2 Framework for Underactuated Hand Analysis

The key components of our framework for analyzing the disturbance response of an underactuated mechanism are: (1) the

<sup>1</sup>Corresponding author.

Contributed by the Mechanisms and Robotics Committee of ASME for publication in the JOURNAL OF MECHANISMS AND ROBOTICS. Manuscript received January 5, 2011; final manuscript received January 13, 2012; published online April 25, 2012. Assoc. Editor: Frank C. Park.

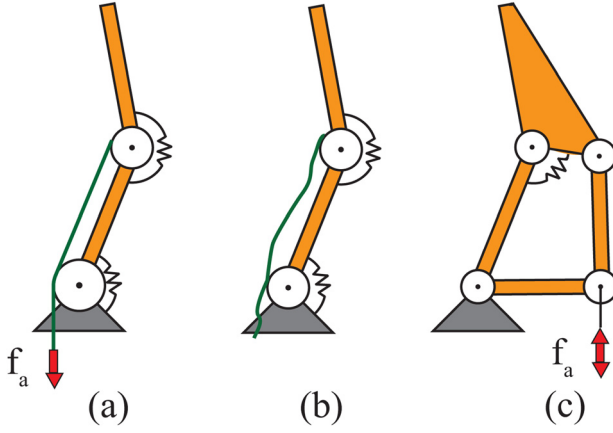


**Fig. 1** Examples of underactuated hands: (a) single-acting cable-driven system, (b) single-acting when the coupling breaks down (cable slack), and (c) double-acting linkage-driven system

kinematics of the coupling constraint, (2) the kinematics of contact, and (3) static balance in the presence of actuator and contact constraints. We will use a two-link revolute–revolute finger with a single actuator for this study (see Fig. 2). For simplicity, we consider contact and external disturbances on the distal link only, which is similar to conditions during precision grasping. Indeed, large external disturbances are most likely to occur on the distal link as it is more likely to make contact with objects in the external environment [18].

**2.1 Kinematics of the Coupling Mechanism.** The coupling between an underactuated mechanism’s actuator and the degrees of freedom may be expressed as a first-order differential equation in the mechanism’s configuration  $\theta = \begin{bmatrix} \theta_1 \\ \theta_2 \end{bmatrix}$  and actuator variable  $\theta_a$ . In cable-driven mechanisms, the actuator variable  $\theta_a$  may be defined as the angle traveled by the actuator pulley over which the cable travels, while in linkage-driven mechanisms, the actuator variable  $\theta_a$  may be defined as the angle traveled by the actuating link.

For cable-driven underactuated mechanisms such as the SDM hand, the kinematics of the coupling mechanism may be expressed as

$$d\theta_a = r_1 d\theta_1 + r_2 d\theta_2 \quad (1)$$

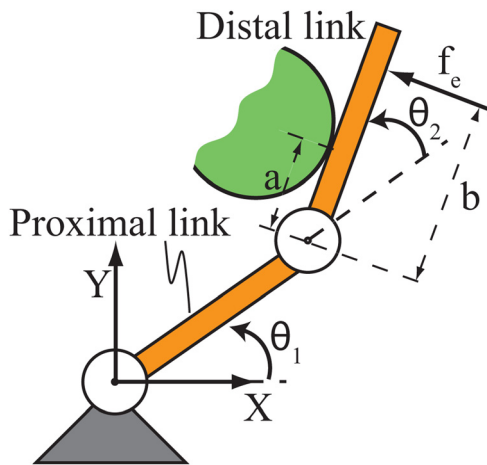


**Fig. 2** A two-link revolute–revolute finger making contact with an object and simultaneously acted on by a disturbance force  $f_e$ . Examples of underactuated mechanisms are shown in Fig. 1.

where  $r_1$  and  $r_2$  represent the pulley radii (assuming unit radius for the actuator pulley).

For four-bar linkage-driven underactuated mechanisms such as the SARAH hand, the kinematics of the coupling mechanism may be expressed as

$$d\theta_a = d\theta_1 + R d\theta_2 \quad (2)$$

where  $R$  represents the transmission ratio of the mechanism. Note that for a four-bar linkage mechanism, the transmission ratio  $R$  is a function of joint configuration  $\theta$  and link lengths. For the instantaneous analysis at a given configuration  $\theta$  in this paper, the transmission ratio  $R$  is treated as a constant.

A closer analysis of Eqs. (1) and (2) shows that the kinematics of both cable-driven mechanisms and linkage-driven mechanisms may be expressed as [18]

$$d\theta_a = J_a d\theta \quad (3)$$

where  $J_a = [a_1 \ a_2]$  represents the mechanism’s actuator Jacobian [19]. For linkage-driven systems,  $a_1$  equals 1 and  $a_2$  equals  $R$ . For cable-driven systems,  $a_1$  equals  $r_1$  and  $a_2$  equals  $r_2$ . For both types of systems, the transmission ratio may be defined as  $R = a_2/a_1$ .

The kinematic representation (3) of the coupling mechanism makes it straightforward to study different mechanisms such as nonbackdrivable systems, where the actuator position is fixed unless it is driven internally, by setting the constraint

$$d\theta_a = 0 \quad (4)$$

The same constraint (4) occurs even in situations where the actuator position is locked intentionally, for example, after the finger reaches a certain configuration. This operation mode, which we term the position-control mode, is a key focus of this paper. The position-control mode is advantageous from a power consumption standpoint since the actuator position may be locked without continuous actuator use.

The common structure of existing underactuation hands’ coupling mechanisms (given by Eq. (3)) induces the hands to behave in a similar fashion when driven internally by the actuator [2]. However, as will be shown, these mechanisms behave differently in the presence of disturbance forces.

**2.2 The Kinematics of Contact.** The contact that occurs between the robot finger and the object during the grasping process imposes additional constraints on the motion of the finger. In this paper, we assume for simplicity that the contact point is fixed in space (similar to Ref. [2]), while permitting the contact point on the distal link to slide when static friction is overcome. This condition is similar to a situation where the object is held stationary by ground friction or other fingers as the finger slides on the object. By differentiating the X and Y coordinates of the contact point with respect to the variables representing joint configuration and the contact location on the distal link, the contact constraints may be expressed as

$$J_c \begin{bmatrix} d\theta_1 \\ d\theta_2 \\ da \end{bmatrix} = 0 \quad (5)$$

where

$$J_c = \begin{bmatrix} -l_1 s_1 - a s_{12} & -a s_{12} & c_{12} \\ l_1 c_1 + a c_{12} & a c_{12} & s_{12} \end{bmatrix} \quad (6)$$

represents the contact Jacobian,  $s_i = \sin \theta_i$ ,  $c_i = \cos \theta_i$ ,  $s_{12} = \sin(\theta_1 + \theta_2)$ ,  $c_{12} = \cos(\theta_1 + \theta_2)$ ,  $a$ , the distance of the contact

location from the distal joint, and  $l_1$ , the proximal link length. Note that each row of  $\mathbf{J}_e$  is associated with a contact force  $\lambda_e = \begin{bmatrix} \lambda_x \\ \lambda_y \end{bmatrix} \in \mathbb{R}^2$  that represents the interaction forces in the X and Y directions required to maintain contact. These contact forces in the X and Y directions can be mapped to the distal link's tangential and normal directions as

$$\begin{bmatrix} \lambda_n \\ \lambda_t \end{bmatrix} = \begin{bmatrix} c_{12} & -s_{12} \\ s_{12} & c_{12} \end{bmatrix} \begin{bmatrix} \lambda_x \\ \lambda_y \end{bmatrix} \quad (7)$$

which indicate the tangential and normal contact forces required to maintain contact. Note that the finger maintains contact with the object only when the normal contact force is positive. The tangential contact force represents the frictional force required to maintain equilibrium. Note that these contact forces are different from the disturbance force,  $f_e \in \mathbb{R}$ .

**2.3 Static Balance in the Presence of Actuator and Contact Constraints.** Once the robotic hand is placed in a specific configuration through internal actuation, an external disturbance force,  $f_e \in \mathbb{R}$ , can cause the robotic hand to change configuration. The external force could be applied, for example, by the other fingers through the object. The magnitude and direction of  $d\theta$  in the joint configuration space depends on factors such as (1) the coupling mechanism, (2) the direction, magnitude, and location of the disturbance force (considered positive in the flexion direction), (3) joint stiffness, (4) the hand control mode, and (5) the contact constraints. This section describes the change in robot configuration as a function of all five factors (assuming disturbance forces normal to the links).

The configuration change  $d\theta$  for an external force  $f_e$  can be quantified using a Lagrangian view of the work done by the external forces and the energy stored in the springs in the presence of the actuation and contact constraints [20]. Specifically, we can define the Lagrangian  $L \in \mathbb{R}$  as

$$L = dW_s + dW_e + dW_a + dW_c \quad (8)$$

where  $dW_s$  represents the work done on the springs,  $dW_e$  the work done by the external forces,  $dW_a$  the work done on the actuator, and  $dW_c$  the virtual work done at the contact location.

The work done on the spring  $dW_s = -1/2 d\theta^T \mathbf{K}_j d\theta$  and the work done by the external forces  $dW_e = f_e (\mathbf{J}_e \cdot d\theta)$  [21] are similar in form for all of the underactuated mechanisms we consider. Here,

$\mathbf{K}_j = \begin{bmatrix} K_1 & 0 \\ 0 & K_2 \end{bmatrix}$  represents joint stiffness, and

$$\mathbf{J}_e = [b_2 + l_1 \cos \theta_2 \quad b_2] \in \mathbb{R}^2 \quad (9)$$

the disturbance force Jacobian that maps external disturbances to joint torques [2]. While this formulation assumes that the external disturbance can slide on the link without friction, friction

models can also be incorporated to represent disturbance forces of arbitrary direction.

If the finger makes contact with an object (see Sec. 2.2), the virtual work at the contact location given by  $dW_c = (\lambda_c - \lambda_{c0})^T (\mathbf{J}_c d\theta)$  must equal zero [22], where  $\lambda_{c0} = \begin{bmatrix} \lambda_{x0} \\ \lambda_{y0} \end{bmatrix}$  represents the contact force in the X and Y directions to maintain stability prior to the application of external disturbance  $f_e$ .

The work done on the actuator  $W_a$ , however, takes different forms depending on the control mode the mechanism is operated in (see Table 1). In the force-control mode (that is, actuator force is controlled to be constant while actuator position can vary), the work is “real.” In contrast, if the robot is in position-control mode (that is, the actuator position is held fixed and the actuator force can vary, (4)), the “virtual” work must equal zero [22]. In the work equation for the position-control mode,  $p$  is the pretension in the actuating mechanism that ensures mechanism stability prior to the application of external disturbance  $f_e$ .

By taking derivatives of the Lagrangian with respect to the variables and any Lagrange multipliers, we can derive the static balance equations for each control mode [20] (see Table 1).

A closer look at the static balance equations reveals that the system response in the decoupled mode (that is, the actuator applies no load or position constraint, such as the case when a tendon goes slack) is shaped primarily by the joint stiffnesses  $K_1$  and  $K_2$ . The system response in the force-control mode is shaped by the joint stiffnesses  $K_1$  and  $K_2$ , the constant actuation force  $f_a$ , and pulley radii  $r_1$  and  $r_2$ . Thus, the system response in the force-control mode may be viewed as a modified version of the system response in the decoupled mode, since the only difference is the work done on the actuator. The performance of underactuated mechanisms in force-control mode has been analyzed in depth in prior work (even in the presence of contact constraints) [2], but an explicit analysis of their disturbance response has not been done.

The system response in the position-control mode without contact is shaped by the joint stiffnesses  $K_1$  and  $K_2$  and the pulley radii ratio  $R$  (due to the actuator position constraint), and the actuator pretension  $p$ . The position-control constraint (4) implies that the proximal and distal-joint configuration changes are opposite in sign for external disturbance forces (if the mechanism can move). Also, the disturbance forces can affect the internal coupling force, and even cause it to become zero and nullify the actuator constraint in the case of a single-acting mechanism. Then, the mechanism transitions from the “position-control mode without contact” state to the “decoupled mode” state. Thus, the static balance for a single-acting mechanism in position-control mode represents a hybrid system where the response can be significantly different under different conditions.

Interestingly, the system is immobile in position-control mode in the presence of contact (see Table 1). Specifically, the three constraints, namely, fixed actuator position and the contact constraints in Eq. (5), prevent any reconfiguration for any external disturbance forces. The only effect of the disturbance force is to

**Table 1 Static balance equations for underactuated mechanisms under different conditions**

Actuation mode	Work done on actuator $dW_a$	Static equations	Example scenario
Force control without object contact	$f_a d\theta_a$	$Kd\theta + J_e^T f_e + J_a^T f_a = 0$	Maintaining fixed cable tension in SDM hand
Position control without object contact	$(\lambda_a - p)d\theta_a = 0$	$J_a d\theta = 0$ $Kd\theta + J_e^T f_e + J_a^T (\lambda_a - p) = 0$	Maintaining fixed cable length in SDM hand and nonbackdrivability in SARAH hand
Position control with distal object contact	$(\lambda_a - p)d\theta_a = 0$	$J_a d\theta = 0$ $J_c d\theta = 0$ $Kd\theta + J_e^T f_e + J_a^T (\lambda_a - p) + J_c^T (\lambda_c - \lambda_{c0}) = 0$	The mechanism is placed in position-control mode after making contact with the object

**Table 2 Fixed parameters**

Parameter	Value
Proximal joint stiffness, $K_1$	1 Nm/rad
Proximal and distal link length, $l_1$ and $l_2$	0.1 m
Proximal pulley radius, $r_1$	0.02 m
Pulley radius ratio, $R = r_2/r_1$	0.6
Proximal joint configuration, $\theta_1$	$\pi/10$ rad
Distal-joint configuration, $\theta_2$	$\pi/3$ rad
Cable pretension, $p$ (when present)	10 N

modify the internal coupling force and the contact forces. Note that certain disturbance forces can cause any one of the constraints to break, depending on the pre-existing conditions (namely cable pretension  $p$  and pre-existing contact forces  $\lambda_{c0}$ ). Once a constraint is broken, the mechanism can reconfigure subject to the remaining constraints, again indicating that the static balance for an underactuated mechanism in contact is also a hybrid system.

It is straightforward to interpret the mechanism's reconfiguration as the mechanism's compliance  $C$  at the contact point

$$C = dh/f_e \quad (10)$$

where  $dh \in \mathbb{R}$  represents the deviation of the disturbance force location in the force's direction  $\mathbf{v} = \begin{bmatrix} s_{12} \\ -c_{12} \end{bmatrix}$ .

### 3 Results

We use the SDM hand [23] as an exemplar of a single-acting mechanism and the SARA hand [9] as an exemplar of a double-acting mechanism to present the results from the simulations of the models presented in Sec. 2. The results focus on three aspects of the disturbance response: mechanism reconfiguration, contact force variation, and actuator force variation. Sections 3.1 and 3.2 explore mechanism reconfiguration and compliance in the absence of contact. Section 3.3, however, explores the variation in the contact forces and actuator forces in the presence of object contact. Table 2 shows the set of parameters that were used in this analysis.

**3.1 Mechanism Reconfiguration Due to Disturbance in the Absence of Object Contact.** The contour plots shown in Fig. 3 illustrate the change in distal-joint configuration  $d\theta_2$  of a two-link mechanism as a function of the magnitude and direction of

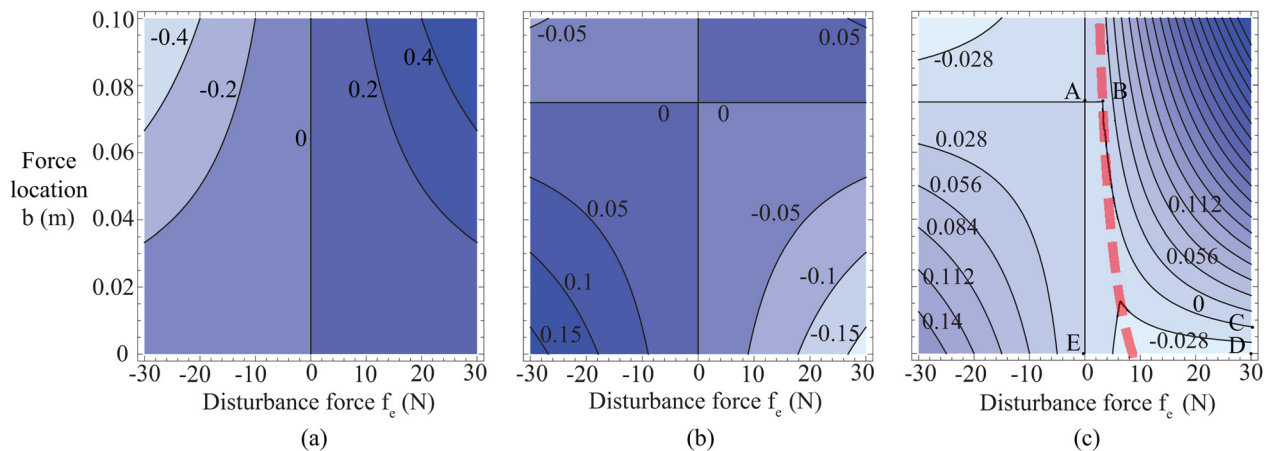
the disturbance force (horizontal axis) and the disturbance force location (vertical axis) in the absence of contact. Note that similar contour plots can be derived for the change in proximal joint configuration  $d\theta_1$ .

Figure 3(a) shows the results for a decoupled system. As expected, the distal joint closes in ( $d\theta_2$  positive) for flexion external forces and opens out ( $d\theta_2$  negative) for extending external forces. The proximal link's behavior is also qualitatively similar, but the exact values will depend on the proximal joint stiffness. The system response in force-control mode is similar to the system response in the decoupled mode, except that the constant actuator force gives a small offset to the contour magnitudes. Due to the relative simplicity of the force-control response behavior, the rest of this paper will focus on the response in position-control mode.

The configuration change is significantly different for a double-acting mechanism in position-control mode (see Fig. 3(b)). Here, we see a critical disturbance force location  $b$  at which the mechanism does not move ( $d\theta_2 = d\theta_1 = 0$ ) for any external force, indicating that the mechanism is very stiff when the disturbance force is applied at that location. This location has been termed the equilibrium point for the mechanism in prior work [2,24]. We also see that the direction of distal-joint motion for the same disturbance force changes depending on whether the disturbance force is located proximal or distal to the equilibrium point. The equilibrium point may be considered as a point about which the distal link pivots when it reconfigures due to a disturbance force.

The equilibrium point is a function of the mechanism design parameters such as proximal link length  $l_1$ , the pulley radii ratio  $R$ , and distal-joint angle  $\theta_2$ , and has the form  $e = l_1 R \cos \theta_2 / (1 - R)$ . This indicates that the equilibrium point could be beyond the distal link tip as the transmission ratio approaches unity. In contrast, the equilibrium point moves proximal on the distal link as the pulley radii ratio  $R$  decreases toward unity, indicating that the equilibrium point could be below the distal joint.

Figure 3(c) shows the distal-joint configuration change  $d\theta_2$  for a single-acting mechanism in position-control mode. The system response is a hybrid between the behavior in decoupled mode (right of the dashed line) and the behavior of a double-acting mechanism in position-control mode (left of the dashed line) seen in Figs. 3(a) and 3(b). The dashed line represents the combination of disturbance force magnitude  $f_e$  and location  $b$  at which the internal coupling breaks down (for example, the cable going slack in the SDM hand). This dashed line is a function of the tendon pretension ( $p = 10$  N in this example), and would lie on the  $f_e = 0$  line if the pretension  $p$  was zero.



**Fig. 3 Disturbance response of a two-link finger in (a) decoupled mode and (b) in position-control mode with a double-acting mechanism. (c) Disturbance response of a two-link finger in position-control mode in a single-acting two-link hand. The contours show variation in distal-joint deviation  $d\theta_2$  as a function of disturbance force  $f_e$  and its location  $b$ . The ratio of joint stiffnesses  $K_r = K_2/K_1$  had a value of 5 in this analysis.**

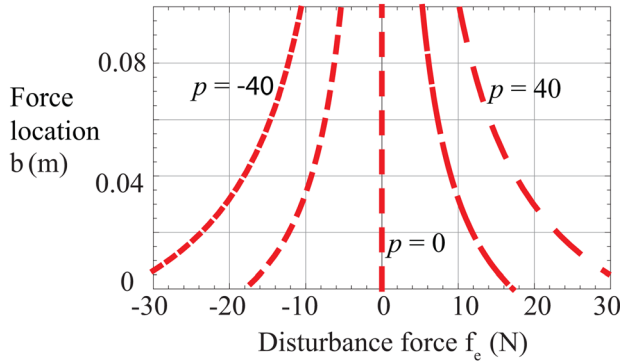


**Fig. 4** Contact force and location combinations that nullify the pretension  $p$  in the actuator

The transition from a position-control mode to a decoupled mode produces interesting behavior when either the disturbance force  $f_e$  or its location  $b$  is small (region ABCDE in Fig. 3(c)). The distal-joint reconfiguration goes from flexion to extension to flexion in a small force range with force location  $0.04 \text{ m} < b < 0.075 \text{ m}$ . As a result, there exists a  $d\theta_2 = 0$  contour to the right of the dashed line also.

Figure 4 shows the combination of disturbance force on the distal link and its location that nullifies a pre-existing internal coupling force (varied here between  $p = -40 \text{ N}$  and  $p = 40 \text{ N}$ ). Note that pretension can be positive or negative for double-acting systems, but can be either only positive or only negative for single-acting mechanism. The contours in this plot are similar to the dashed red line in Fig. 3(c).

**3.2 Mechanism Compliance in the Absence of Object Contact: Variation With Design Parameters.** Using Eq. (10), we can compute the compliance of both a single-acting and double-acting underactuated mechanism at the disturbance force

location. Figure 5 shows the variation in compliance of a double-acting mechanism in position-control mode. We now analyze the variation in compliance across the rows and columns of the subfigures to study the effect of the joint-stiffness ratio  $K_r$  and the distal-joint configuration  $\theta_2$ . As expected, as the joint-stiffness ratio increases from  $K_r = 0.5$  to  $K_r = 10$ , the overall compliance decreases. It is interesting to note that the equilibrium point does not vary with the joint-stiffness ratio  $K_r$ .

As the distal-joint configuration  $\theta_2$  increases from  $\theta_2 = \pi/6$  to  $\theta_2 = \pi/3$ , the compliance also decreases. This is expected because the moment arm of a normal force on the distal link about the proximal joint decreases as the distal-joint angle  $\theta_2$  increases. An interesting aspect not shown in these plots is that the equilibrium point curve shifts rapidly towards the  $b = 0$  and  $R = 1$  locations as the distal link approaches the perpendicular configuration ( $\theta_2 = \pi/2$ ). This indicates that at large flexion angles, the mechanism exhibits large stiffness only when the normal disturbance force is very close to the distal joint or when the pulley radius ratio  $R$  is close to unity. The condition  $R = 1$  is particularly interesting, since in this situation the proximal joint motion is exactly opposite to the distal-joint motion, causing the distal-joint configuration to be fixed relative to a world coordinate frame.

For extension disturbance forces, a single-acting mechanism like the SDM hand in position-control mode behaves identical to the double-acting mechanism since the coupling constraint is active (see Fig. 5). However, a single-acting mechanism in position-control mode exhibits bimodal compliance for a flexion disturbance force (see Fig. 6), depending on if the internal coupling is active. Indeed, a large enough flexion force can cause the internal coupling force to become zero, rendering the coupling constraint inactive. These results are similar to those seen in Fig. 3(c).

In Fig. 6, the thin (red) lines in the left region represent the compliance contours when the joints are still coupled, and the compliance behavior of the single-acting mechanism is identical to the compliance of a double-acting mechanism in this region. However, certain parameter combinations (indicated by the solid

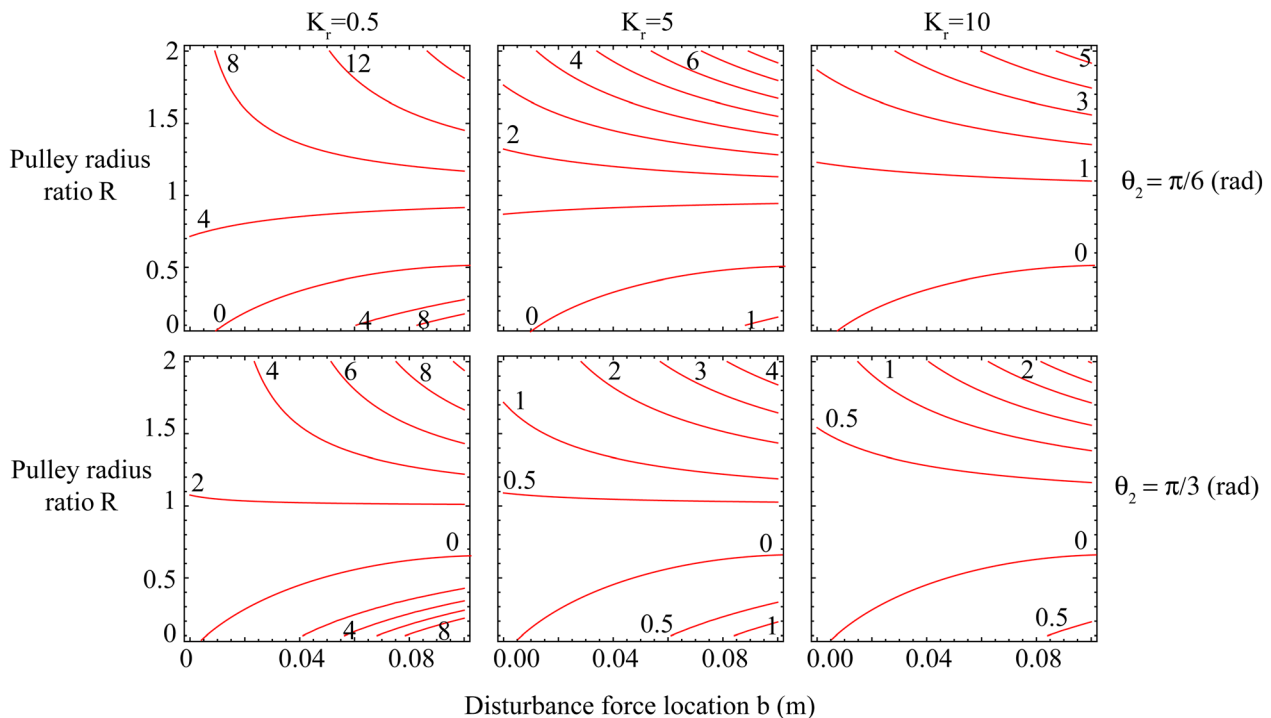


**Fig. 5** Variation of the compliance (mm/N) of an underactuated mechanism with an active coupling constraint (such as in a double-acting mechanism). The parameters explored are distal link configuration  $\theta_2$ , joint-stiffness ratio  $K_r$ , the pulley radius ratio  $R$ , and disturbance force location  $b$ . The joint-stiffness ratio  $K_r$  increases from left to right across the subfigures and the joint angle  $\theta_2$  increases from top to bottom across the subfigures. The disturbance force  $f_e$  had a value of 5 N in this analysis.

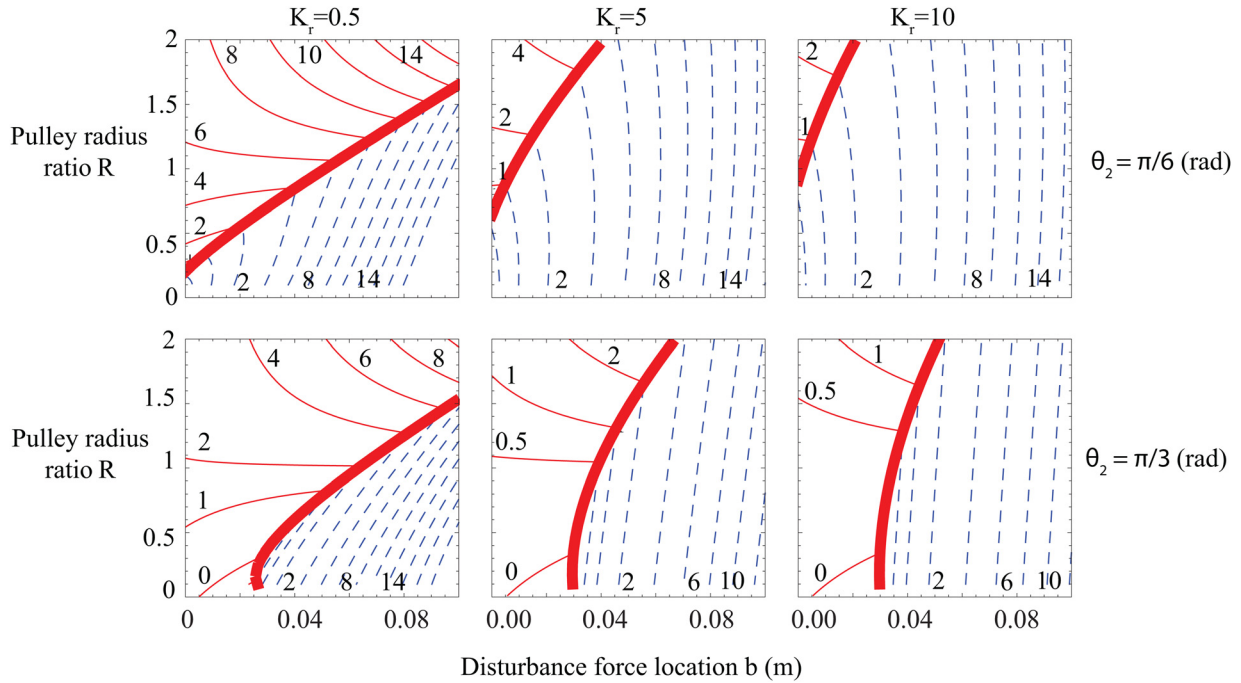


**Fig. 6** Variation of the compliance (mm/N) of an underactuated mechanism where the coupling constraint can become inactive (such as in a cable-driven single-acting mechanism in position control mode). The parameters explored are distal link configuration  $\theta_2$ , joint stiffness ratio  $K_r$ , pulley radius ratio  $R$ , and distal force location  $b_2$ . The joint-stiffness ratio  $K_r$  increases from left to right across the subfigures and the joint angle  $\theta_2$  increases from top to bottom across the subfigures. The thick solid line represents the parameter combinations at which the mechanism transitions into the decoupled mode. The thin lines represent parameter combinations at which the joints are coupled, and the dotted lines represent parameter combinations at which the joints are completely decoupled. The disturbance force  $f_e$  had a value of 5 N in this analysis.

red line) can render the coupling constraint inactive. The parameter space to the right of this line represents the region when the joints are decoupled. Note that the boundary between these regions is a function of the pretension  $p$  in the system and shifts to the right as the pretension increases.

We notice that the compliance is generally higher in the decoupled region when compared with the region when the joints are coupled. This is expected since most of the stiffness for the underactuated mechanism in position-control mode comes from the coupling mechanism. Also, the variation of mechanism compliance with pulley radius ratio  $R$  in the decoupled state is much lower than in the coupled state. While one may have expected the decoupled compliance to be independent of pulley radius ratio  $R$ , the single-acting mechanism actually transitions from a constraint-active state to a decoupled state. Thus, the effect of pulley radius ratio  $R$  on compliance in the constraint-active state carries over to the effective compliance even in the decoupled state.

**3.3 Trade-offs in Object Contact Forces and Actuator Forces Due to Disturbance.** As discussed in Sec. 2.3, a two-link underactuated mechanism in contact with an object and placed in position-control mode is immobile to external disturbances. Also, when the finger makes contact with the object during the grasping process, the initial contact force  $\lambda_{c0}$  and actuator force  $p$  magnitude may be volitionally set before the mechanism is placed in position-control mode.

However, the disturbance forces do affect the contact force and the internal coupling force, and this section identifies how the contact location and the mechanism's equilibrium point influence the disturbance response. Note that this analysis applies to both single-acting and double-acting mechanisms since the coupling constraint is assumed to be active initially.

Figures 7(a) and 7(b) show the slopes of the variation in normal contact force and actuator force with respect to a variation in the

disturbance force, that is,  $d\lambda_n/df_e$  and  $d\lambda_a/df_e$  (hereafter, referred to as just "slopes"), as a function of the disturbance force location. If the disturbance force produces a large moment, then it can cause one of the constraints to break down. Specifically, looking at Fig. 7(a), a positive disturbance force acting at  $b = 0.02$  m would cause both the normal contact force and the actuator force to increase. A negative disturbance force would cause the normal contact force and the actuator force to decrease. For a large enough (negative) disturbance force, the contact force could become zero in which case the finger loses contact with the object and the contact constraint becomes inactive. Note that in a double-acting mechanism, the coupling constraint would always be active even if the internal coupling force became negative.

However, for a single-acting mechanism, the internal coupling force could become zero and cause the mechanism to enter the decoupled state (with contact). Interestingly, the slopes of the normal contact force and the internal coupling force are different and thus, which constraint first becomes inactive depends on the initial values of the normal contact force and the actuator force. Thus, the initial conditions and the disturbance determine which constraints breaks first. This is important since it determines how the mechanism subsequently reconfigures.

The slopes change with the disturbance force location as well. If the disturbance force acts at the contact location, then the actuator force does not change (actuator force slope is zero), but the normal contact force increases with unit slope. If the disturbance force acts at the equilibrium point, then the contact force does not change (contact force slope is zero), but the actuator force increases proportionally. For other disturbance force locations, the slopes change at different rates. Section 4.2 offers insight into how the slopes vary with the location of the disturbance force relative to the contact point and the equilibrium point.

From this analysis, we notice that the hybrid nature of the static balance in the presence of actuation and contact constraints

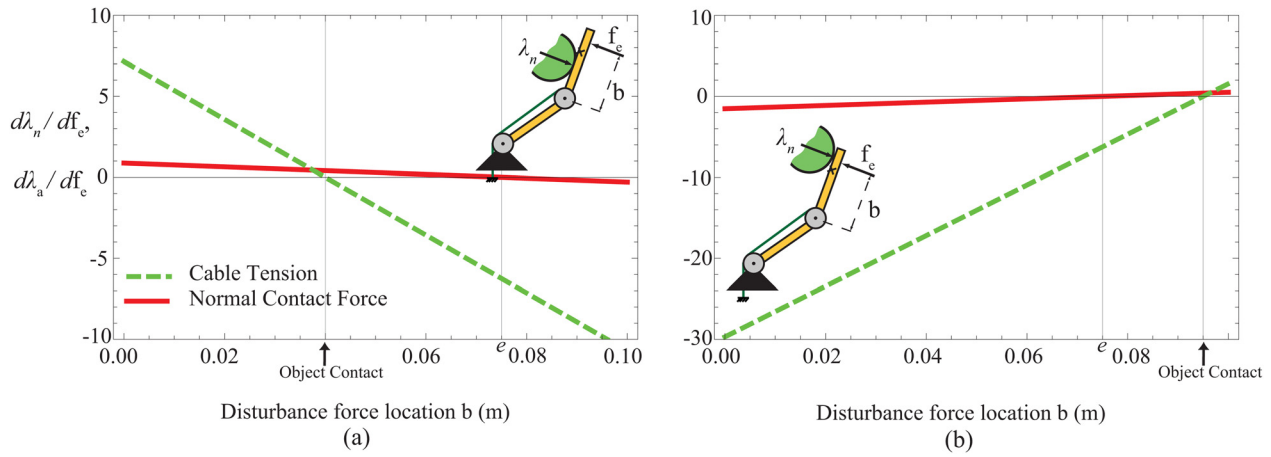


**Fig. 7** Ratio of external force magnitude to the change in object contact normal force and actuator force for object contact on each side of the equilibrium point. The equilibrium point  $e$  is indicated by  $\times$  in the inset figure and the object location constraint is proximal to the equilibrium point in the (a) and distal in (b).

greatly influences mechanism behavior. Section 4 provides an analysis of how this behavior of underactuation mechanisms influences grasping performance.

#### 4 Discussion

To our knowledge, the only previous study of the disturbance response of underactuated mechanisms focused on the whole-hand response to a constant force acting on the object for a specific double-acting mechanism. In this paper, we have identified key differences in the response of underactuated mechanisms that arise from the coupling mechanism and the operational control mode. Most previous studies of underactuated hands have explored design issues focused on favorable behavior when the actuator force is controlled [1–5]. Even though we consider only a simple two-link finger in this paper, a close analysis in position-control mode provides insight into the behavior of general underactuated mechanisms.

The discussion focuses on four aspects of the external disturbance response of underactuated mechanisms: (1) the grasping behaviors exhibited in the absence of object; (2) the role played by the equilibrium point on the object contact forces; (3) exploiting the robot design parameters to improve the disturbance performance; and (4) limitations of the current analysis.

**4.1 Grasping Behaviors Resulting From Mechanism Reconfiguration in the Absence of Object Contact.** When an underactuated mechanism is not fully constrained due to the contacts with the environment, external forces will cause it to reconfigure. This reconfiguration can lead toward either increased or decreased grasping ability, depending on the joint motions. Figure 8 shows the general joint configuration change space for any two-link finger for a nominal configuration. Note that this figure only shows the space of relative joint angle changes that might happen due to reconfiguration at the nominal configuration and is not a function of disturbance force or actuation mode. The regions represent four grasp behaviors, (1) squeeze, (2) cage, (3) eject, and (4) release, which are all described in Table 3. These regions are based on the direction of potential fingertip movement in the X-direction (the red solid line) and proximal joint configuration change for the nominal configuration. The (red) solid line in Fig. 8 indicates reconfigurations where the tip motion in the X-direction is zero (given by reconfigurations that satisfy  $(l_2s_{12})d\theta_2 + (l_1s_1 + l_2s_{12})d\theta_1 = 0$ ) and is a function of finger configuration and finger length parameters. Prior work in grasping has also explored the eject [2,25] (albeit in a different form), cage [26–29], and hold [30] behaviors.

Unfortunately, there is no accepted metric in the literature for ranking the utility of such grasp acquisition behaviors. In this paper, we use a simple yet novel method for qualitatively ranking grasp behaviors. Assuming an object with circular cross section and the goal of increasing the potential for contact with the object, we rank the various grasping behaviors in decreasing order of preference as squeeze, cage, eject, and release.

The coupling mechanism in underactuated fingers precludes the possibility of arbitrary configuration change. In force-control mode or the decoupled mode, the direction of motion of the proximal joint and distal joint would be identical, indicating a positive slope in the joint configuration space. Figure 9(a) shows an interpretation of the contour plots shown in Fig. 3(a) as grasp behaviors, with each region corresponding to a particular grasp behavior for the decoupled mode.

Interesting behaviors arise when the mechanism is operated in position-control mode. An active coupling constraint enforces the proximal and distal joints to move in opposite directions. Interestingly, if the pulley radius ratio  $R$  is less than 0.61, then the mechanism exhibits only cage and eject behaviors under

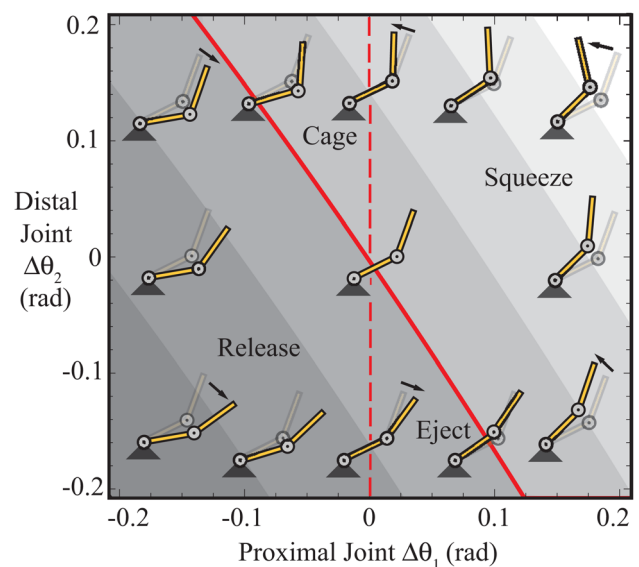


**Fig. 8** Grasping behaviors of a two-link finger as a function of joint deflection. The fingertip has displacement along the negative X direction in the region to the right of the red solid line.

**Table 3 Robot hand behaviors and potential effect on a grasp**

Behavior	Fingertip and joint motions	Potential effect on grasp acquisition
Squeeze	Negative X-motion; both joints curl in	Envelops object; potential for multiple contacts
Caging	Negative X-motion; distal joint curls inward, proximal joint opens	Envelops object with potential distal contact
Ejection	Positive X-motion; proximal joint curls, distal joint opens	Potential contact with proximal phalanx, but distal joint moves outward. Potential for losing object from grasp
Release	Positive X-motion; both joints open	Potential for contact at both links decrease

position-control mode at the chosen nominal configuration. If the pulley radius ratio  $R$  is greater than 0.61, then the mechanism exhibits only squeeze and release behaviors under position-control mode at the chosen nominal configuration. Furthermore, Figure 9(b) shows that the grasping behavior is a function of the direction and location of the external force (for  $R = 0.6$ ).

The position-control constraint can break down in single-acting mechanisms (due to the cable becoming slack, for instance), and thus they exhibit a bimodal behavior to external disturbances, in contrast to double-acting mechanisms which offer a smooth variation in response in position-control mode. As shown in Fig. 9(c), we notice that the single-acting mechanism exhibits cage, eject, and squeeze behaviors at the nominal configuration, depending on the disturbance force.

Interestingly, hands with single-acting mechanisms produce an ejection behavior for small external loads (region ABCDE in Fig. 3(c)), but transition into squeeze behavior for larger forces. If the eject behavior for small loads (region ABCDE) is to be eliminated in cable-driven systems (since it is less preferred than the squeeze behavior), we infer from Figs. 3(c) and 4 that the pretension must be zero. In such a condition, any flexion load will cause the mechanism to enter the squeeze behavior. However, a zero pretension in the actuation mechanism is not always possible, particularly when the hand is already applying forces to a grasped object. The key aspect of the single-acting mechanism is that it naturally complies with external forces when the coupling constraint becomes inactive. Thus, the single-acting mechanism is better than a double-acting mechanism during the grasping process at this nominal configuration, since the eject behavior region of the single-acting mechanism is smaller than the eject behavior region for a double-acting mechanism. Indeed, proper choice of coupling ratio (and subsequent equilibrium point) can put the upper eject region off of the link, and minimizing the tendon tension can minimize the lower region, thus making nearly all possible disturbance forces result in desirable cage or squeeze behaviors.

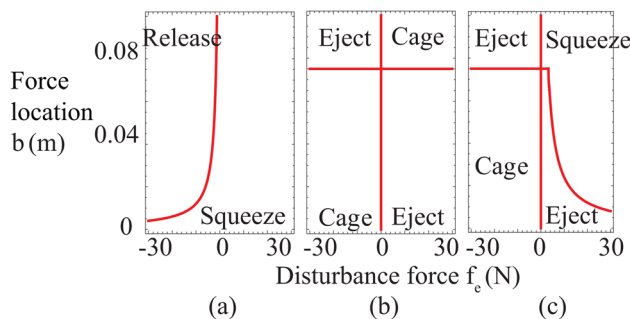


**Fig. 9 Disturbance response behavior of two-link finger in (a) force-control mode, (b) double-acting position-control mode, and (c) single-acting position-control mode**

**4.2 The Effect of Disturbances and the Equilibrium Point on Grasp Contact Forces.**

Section 3.3 showed that the change in object contact force in relation to the external disturbance was largely a function of disturbance force location and the relationship between the equilibrium point and the contact location. The key factor in determining the sign of the slopes for both actuator force and the normal contact force is the point about which the distal link pivots instantaneously. Specifically, in Fig. 7(a), if the disturbance force acts proximal to the contact location, then the distal link pivots about the contact location, causing the actuator forces and contact forces to increase for positive disturbance forces. In contrast, if the disturbance force acts distal to the equilibrium point, then the distal link pivots about the equilibrium point, causing the actuator forces and contact forces to decrease for positive disturbance forces. For disturbance forces applied at in-between locations, the slopes differ accordingly. Interestingly, Figs. 7(a) and 7(b) also indicate that the relative position of the equilibrium point and the contact location also influences the slopes since the pivot point differs.

Since the stability of an object within a grasp is a function of contact forces, a decreasing contact force is undesirable. For example, Fig. 7 shows that even flexion disturbances can cause the normal contact force to decrease in position-control mode. Although not shown in Fig. 7, a decoupled single-acting system will generate an increase in object normal force for all flexion disturbances located on the distal link. For this reason, the breakdown in coupling constraint seen in single-acting systems can ameliorate the effects of external disturbances on object contact forces.

**4.3 Design of Underactuated Hands.**

A key result in this paper is identifying the parameter space where the coupling constraint becomes inactive in single-acting mechanisms. The constraint becoming inactive in an underactuated mechanism does have benefits, as it provides a desirable disturbance rejection behavior by yielding to the external disturbance force by curling in naturally and improving the grasp potential (see Fig. 10(a) where the finger envelopes the object). In contrast, a double-acting mechanism where the constraint is always active exhibits complex reconfiguration which can negatively influence a grasp (see Figs. 10(b) and 10(c) where only one link closes in on the object).

The parameter space where the coupling constraint becomes inactive increases for lower pretension values, suggesting that pretension should be kept as small as possible to ensure a natural curling to external disturbances (see Fig. 6). Also, this parameter subspace increases with larger joint-stiffness ratio  $K_r$ . This accords with previous results that showed that the distal joint should be much stiffer than the proximal joint in order to retain a desirable hand grasping configuration in the presence of object contact forces [31]. Independently, it has also been shown that a higher joint-stiffness ratio  $K_r$  helps in grasp stability as well [32].

The equilibrium point has been used in previous work as the point toward which a precision grasp's contacts slide (when internally actuated) for the grasp to become stable [2]. Thus,

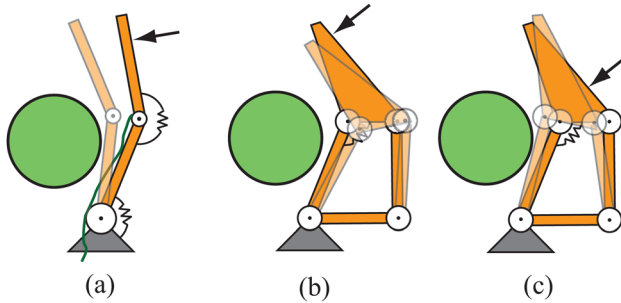


**Fig. 10** Disturbance response in position-control mode of (a) a single-acting mechanism where the coupling constraint becomes inactive (cable slackens). The mechanism complies naturally with the disturbance force and curls in. (b) Double-acting mechanism showing caging behavior in response to disturbance force. (c) Double-acting mechanism showing eject behavior in response to disturbance force.

underactuated hands have been designed to locate the equilibrium point within the distal link, without which the object may be ejected. From our analysis of the response of the fingers to external disturbance (see Figs. 9(b) and 9(c)), we notice that another aspect of the equilibrium point may be exploited as well. Both the double-acting and single-acting mechanisms in position-control mode transition between different behaviors (cage and eject in this instance) at the equilibrium point. Thus, the finger could be designed to place the equilibrium point so as to maximize the areas of desired motion across the mechanism's joint configuration space. More work is required to provide a unified view of underactuated grasping in the light on internal actuation and external disturbances.

It is also interesting to note that since the joint stiffnesses do not affect the equilibrium point, they can be chosen based on other factors. For instance, the ratio of the joint stiffnesses can be set in order to ensure that the proximal joint closes in on an object at a faster rate than the outer joint when actuated to ensure maximum grasping ability in the presence of uncertainty [33].

**4.4 Limitations of Current Analysis.** During the grasping process, a robotic finger experiences a variety of disturbance forces as well as contact constraints (rolling and sliding on the object). In this paper, we have used a simple contact model where the contact location is fixed in a spatial frame, used normal disturbance forces that act only on the distal link and change orientation with it, and assumed sufficient frictional forces. The primary reason is to focus on the interesting bimodal disturbance response of the single-acting mechanism in position-control mode through an instantaneous quasi-static analysis, which to our knowledge has not been explored before. Note that the fixed contact point model is similar to the situation when the object is held fixed by ground friction or the other fingers, and the moving disturbance force is also similar to the forces acting on the finger through the object.

## 5 Conclusion

In this paper, we have presented, to our knowledge, the first analysis of single-acting and double-acting underactuated mechanisms that focuses on the differences in the behaviors exhibited in the presence of external disturbances. While both systems utilize clever adaptive mechanisms that couple the motion of the actuator and joints in nominal conditions, the coupling constraint can become inactive in single-acting mechanisms. This produces significantly different joint reconfiguration behaviors in underactuated hands during the process of grasping an object. Using simulation models to study the external disturbance response, we notice that there are advantages to the coupling constraint

becoming inactive, since the single-acting mechanism complies with the external force and thus can adapt to the object shape. Finally, by noticing that the equilibrium point is a critical element that determines these behaviors, we have provided suggestions to exploit the mechanism's parameters to place the equilibrium point to improve performance.

## Acknowledgment

The authors thank Lael Odhner for helpful discussions on Lagrangian formulation of mechanical systems. This work was funded in part by the National Science Foundation Grant No. IIS-0953856 and the Gustavus and Louis Pfeiffer Research Foundation.

## References

- [1] Dollar, A. M., and Howe, R. D., 2006, "A Robust Compliant Grasper via Shape Deposition Manufacturing," *IEEE/ASME Trans. Mechatron.*, **11**(2), pp. 154–161.
- [2] Birglen, L., Laliberté, T., and Gosselin, C., 2008, *Underactuated Robotic Hands*, Springer, New York.
- [3] Hirose, S., and Umetani, Y., 1978, "The Development of Soft Gripper for the Versatile Robot Hand," *Mech. Mach. Theory*, **13**, pp. 351–359.
- [4] Rakić, M., 1989, "Multifingered Hand With Self-Adaptability," *Rob. Comput.-Integr. Manuf.*, **3**(2), pp. 269–276.
- [5] Rovetta, A., 1981, "On Functionality of a New Mechanical Hand," *ASME J. Mech. Design*, **103**, pp. 277–280.
- [6] Kragten, G. A., Kool, A. C., and Herder, J. L., 2009, "Ability to Hold Grasped Objects by Underactuated Hands: Performance Prediction and Experiments," *Proceedings of IEEE International Conference on Robotics and Automation*, pp. 2493–2498.
- [7] Kamikawa, Y., and Maeno, T., 2008, "Underactuated Five-Finger Prosthetic Hand Inspired by Grasping Force Distribution of Humans," *Proceedings of IEEE/RSJ International Conference on Intelligent Robots and Systems*, pp. 717–722.
- [8] Kaneko, M., Higashimori, M., Takenaka, R., Namiki, A., and Ishikawa, M., 2003, "The 100G Capturing Robot too Fast to See," *IEEE/ASME Trans. Mechatron.*, **8**(1), pp. 37–44.
- [9] Gosselin, C., and Laliberté, T., 1996, "Underactuated Mechanical Finger With Return Actuation," U.S. Patent No. 5,762,390.
- [10] Laliberté, T., and Gosselin, C., 2002, "Actuation System for Highly Underactuated Gripping Mechanism," U.S. Patent No. 6,505,870.
- [11] Carrozza, M. C., Suppo, C., Sebastiani, F., Massa, B., Vecchi, F., Lazzarini, R., Cutkosky, M. R., and Dario, P., 2004, "The Spring Hand: Development of a Self-Adaptive Prosthesis for Restoring Natural Grasping," *Auton. Rob.*, pp. 125–141.
- [12] Crowder, R. M., Dubey, V. N., Chappell, P. H., and Whatley, D. R., 1999, "A Multi-Fingered End Effector for Unstructured Environments," *Proceedings of IEEE International Conference on Robotics and Automation*, pp. 3038–3043.
- [13] Crisman, J. D., Kanojia, C., and Zeid, I., 1996, "Graspar: A Flexible, Easily Controllable Robotic Hand," *IEEE Rob. Autom. Mag.*, **3**(2), pp. 32–38.
- [14] Townsend, W. T., 2000, "The Barretthand Grasper—Programmably Flexible Part Handling and Assembly," *Ind. Robot: Int. J.*, **27**(3), pp. 181–188.
- [15] Torres-Jara, E., 2005, "Obrero: A Platform for Sensitive Manipulation," *Proceedings of IEEE-RAS International Conference on Humanoid Robots*, pp. 327–332.
- [16] Balasubramanian, R., Belter, J. T., and Dollar, A. M., 2010, "External Disturbances and Coupling Mechanisms in Underactuated Hands," *Proceedings of ASME International Design Engineering Technical Conference and Computers and Information in Engineering Conference*.
- [17] Balasubramanian, R., and Dollar, A. M., 2011, "Variation in Compliance in Two Classes of Two-Link Underactuated Mechanisms," *Proceedings of the IEEE International Conference on Robotics and Automation*, pp. 3497–3504.
- [18] Krut, S., 2005, "A Force-Isotropic Underactuated Finger," *Proceedings of the 2005 IEEE International Conference on Robotics and Automation*, pp. 2314–2319.
- [19] Merlet, J. P., 2006, *Parallel Robots*, Springer, The Netherlands.
- [20] Inoue, T., and Hirai, S., 2008, *Mechanics and Control of Soft-Fingered Manipulation*, Springer, New York.
- [21] Craig, J. J., 1989, *Introduction to Robotics*. Addison-Wesley, Reading.
- [22] Murray, R. M., Li, Z. X., and Sastry, S. S., 1994, *A Mathematical Introduction to Robotic Manipulation*, CRC Press, Boca Raton, FL, USA.
- [23] Dollar, A. M., and Howe, R. D., 2010, "The Highly Adaptive SDM Hand: Design and Performance Evaluation," *Int. J. Robot. Res.*, **29**(5), pp. 585–597.
- [24] Rizk, R., Krut, S., and Dombre, E., 2007, "Graspstability Analysis of a Two-Phalanx Isotropic Underactuated Finger," *Proceedings of IEEE/RSJ International Conference on Intelligent Robots and Systems*, pp. 3289–3294.
- [25] Begoc, V., Durand, C., Kurt, A., Dombre, E., and Pierrot, F., 2006, "On the Form-Closure Capability of Robotic Underactuated Hands," *Proceedings of the*

- International Conference on Control, Automation, Robotics, and Vision*, pp. 2011–2018.
- [26] Diankov, R., Srinivasa, S., Ferguson, D., and Kuffner, J., 2008, “Manipulation Planning With Caging Grasps,” *Proceedings of IEEE International Conference on Humanoid Robots*, pp. 285–292.
- [27] Vahedi, M., and van der Stappen, a. F., 2008, “Caging Polygons With Two and Three Fingers,” *Int. J. Robot. Res.*, **27**(11–12), pp. 1308–1324.
- [28] Rodriguez, A., and Mason, M. T., 2008, “Two Finger Caging: Squeezing and Stretching,” Workshop on the Algorithmic Foundations of Robotics.
- [29] Rimon, E., 1999, “Caging Planar Bodies by One-Parameter Two-Fingered Gripping Systems,” *Int. J. Robot. Res.*, **18**(3), pp. 299–318.
- [30] Kragten, G. A., and Herder, J. L., 2010, “The Ability of Underactuated Hands to Grasp and Hold Objects,” *Mech. Mach. Theory*, **45**, pp. 408–425.
- [31] Dollar, A. M., and Howe, R. D., 2005, “Towards Grasping in Unstructured Environments: Grasper Compliance and Configuration Optimization,” *Adv. Rob.*, **19**(5), pp. 523–543.
- [32] Ciocarlie, M., and Allen, P., 2009, “A Design and Analysis Tool for Underactuated Compliant Hands,” *Proceedings of the IEEE/RSJ International Conference on Intelligent Robots and Systems*, pp. 5234–5239.
- [33] Dollar, A. M., and Howe, R. D., 2005, “Towards Grasping in Unstructured Environments: Grasper Compliance and Configuration Optimization,” *Adv. Rob.*, **19**(5), pp. 523–544.